MORPHING BLADES WITH EMBEDDED SMA STRIPS: AN EXPERIMENTAL INVESTIGATION

Annalisa Fortini[*], Alessio Suman[**], Mattia Merlin[*], Gian Luca Garagnani[*]

[*]Metallurgy research group, Engineering Department in Ferrara (ENDIF), University of Ferrara, Italy
[**]Fluid machinery research group, Engineering Department in Ferrara (ENDIF), University of Ferrara, Italy

HIGHLIGHTS

- Design of a morphing blade made up of polymeric matrices with embedded NiTi elements
- Development of a specifically designed shape setting treatment
- Comparison of thermoplastic polymeric compounds
- Study of blade changes by digital image analysis and CAD reconstruction
- Innovative 3D actual blade shape detection by means of a non-contact sensor

ABSTRACT

This paper focuses on the development and experimental testing of a composite blade for an automotive axial fan. A novel concept of morphing blade is proposed with the aim of replacing the conventional actuator systems. The structure is made up of a polymeric matrix equipped with NiTi shape memory alloy strips as active elements. The morphing blade changes its shape as the phase transformations of the strips are thermally activated by airflow. To study the morphing capability of the blade, together with the recovery behavior of the NiTi strips, four different polymeric compounds have been compared. Digital image analysis techniques have been performed to quantitatively analyze the blade deflections and to evaluate the most suitable polymeric matrix for the intended application. Finally, the blade shape modifications, which occur along the blade span during the activation cycles, have been reconstructed by three-dimensional non-contact surface detection. Results from the comparison between these two reverse engineering methods could provide a powerful support for the assessment of the aerodynamic performance of the morphing blade.

KEYWORDS: NiTi shape memory alloy, polymeric matrix, adaptive deformable structure, digital image analysis, reverse engineering

INTRODUCTION

The ongoing employment of Shape Memory Alloys (SMAs) elements as solid-state actuators results from the Shape Memory Effect (SME) and the unique mechanical characteristics of these materials, including high reversible strain (up to 10 %), high-power to weight ratio and the ability to generate high recoverable stresses (up to 800 MPa) [1, 2]. The application of smart materials to compact, high-energy density devices as well as the development of modeling and control systems has been of a great interest over the last decade.

SMAs are frequently combined within monolithic or composite host materials to produce adaptive structures of which the properties could be tuned in response to external stimuli. The integration of smart materials in actuation systems represents an excellent technological opportunity and an alternative solution to conventional mechanical systems for the development of mechanisms that are simple, very compact and reliable. Owing to the simplicity of the fabrication of commercial shape memory alloys in the form of wires, fibers, ribbons, particles and thin films, it is possible to develop a great variety of adaptive structures by means of conventional fabrication techniques [3].

This paper focuses on the experimental investigation of a morphing blade for an automotive axial fan. The aim of this study is to assess the capabilities of the blade, which is inherently deformable and adaptable, to change its shape because of SMA phase transformations. Prior to insertion in the polymeric blade structure, the SMA strips were thermally trained through a specifically designed shape setting treatment, enabling blade deflection on heating. Four different thermoplastic matrices were compared to study the recovery behavior of different combinations of the polymeric matrix and SMA strips. SMA phase transformations, achieved by airflow obtained inside a purpose-built wind tunnel, enabled the production of aerodynamic changes in the blade shape depending on the airflow temperature. The recovery behavior of each polymeric matrix with SMA strips was studied through digital image analysis techniques. The different compounds were compared by two-dimensional CAD software reconstruction of the blade

tip. Finally, to further study the stabilization of the functional structure for the chosen compound, the three-dimensional blade shape was analyzed through non-contact surface detection.

LITERATURE SURVEY

Owing to large actuation forces and displacements together with high strain outputs, SMAs are frequently employed for the development of hybrid composite structures with adaptation features. Most of these active composite structures are made by directly or indirectly embedding shape memory elements into thermoplastic and thermosetting matrices. The possibility of embedding SMAs into a host medium mainly regards the development of systems in which the shape, elastic moduli, internal stress level and natural frequency of vibration can be optimized to the specific application. To this regard, many authors [5–8] have demonstrated that SMA wires, which have been thermo-mechanically trained, could work as a linear actuator by contracting on heating and recovering their original shape on cooling, providing the shape changing. Moreover, under constrained conditions, the SMA elements work against the elastic stiffness of the host matrix, biasing their strain recovery. Thus, the phase transformation is accompanied by large recoverable transformation strains, which lead to the generation of considerable stresses. For these reasons, several studies [4, 8] deal with SMA elements embedded in composite structures: through implementation inside the polymeric host structure they pull on the skin due to deformation.

The possibility to use SMA elements for morphing structures is particularly attractive for aerodynamic applications where this actuation solution prevents the introduction of flow-disturbing control elements [9, 10]. A great amount of literature has considered the employment of SMAs for actuation purposes [11–14]. Examples of adaptive structures regard the improvement of the global efficiency of aircraft wings [15–17], helicopter blades [18] and wind turbines [19, 20]. The integration of SMA elements into the adaptive structure allows for the saving of space and weight as well as the reduction of complexity of the whole system. Moreover, SMAs are lightweight, large deflection and quick-response actuators ideally suited for reconfigurable airfoil applications [21, 22]. To this regard, many studies [21, 23] have focused on the study of SMAs as linear actuators, to make reconfigurable airfoils that enable an increase in efficiency of the wing in flight at several different flow regimes. Recently, Sofla *et al.* [16] proposed the design of a shape-morphing wing for small aircrafts which takes advantage of an antagonistic SMA-actuated flexural structural device that enables the wing profile to change by bending and twisting. More recently, the Boeing Company developed an SMA-actuated morphing aerostructure, called Variable Geometry Chevron (VGC), to reduce noise during take-off and to increase cruise efficiency [24]. For these reasons, the notion of smart advanced blades, which can control themselves and reduce (or eliminate) the need for an active control system, is an appealing solution in blade technology.

This paper is arranged according to the following points: (i) blade structure development comprising SMA strip characterization and polymeric compound selection, (ii) thermal activation of the blade through experimental tests, (iii) comparison of the different couplings of the polymeric matrix with SMA strips by means of two-dimensional analysis technique and (iv) three-dimensional non-contact blade detection to reconstruct the blade shape deformations obtained by the action of the SMA strips.

BLADE STRUCTURE DEVELOPMENT

The morphing blade design was performed to create an adaptive structure of which the thermal activation would provide the adjustment of the working condition parameters of the axial fan. The adaptive structure included the polymeric matrix, which ensured the structural integrity of the blade, and the embedded strips, which were the actuator elements, thermally activated by hot/cold airflow. The structure was designed in order to be sufficiently compliant and flexible to support the large deflections induced by the strips and to allow shape recovery, but was also stiff enough to withstand the aerodynamic loads.

The blade sketch with the essential region is reported in Fig. 1. SMA elements were housed inside purpose-built slots in direct contact with the airflow, as depicted in the close-up. As can be seen, the strips were located in the range of about (50 – 85) % of the blade span and, starting from the midchord, in such a way that their shape modification made a camber curvature variation of the airfoil. Conversely, the region near the root is depicted as fixed since no actuation elements were placed there.

SMA strip selection. The choice of the chemical composition of the SMA elements was linked to practical considerations since the best SMA compound must have transformation temperatures as close as possible to those encountered by the fan during operation. For this reason the commercially available NiTi shape memory alloy (Memry Metalle Company), of nominal composition $Ni_{50.2}Ti_{49.8}$ was chosen. Starting from the supplied 1.5 mm thick plate, the strips were cut by means of electro-erosion machining in order to minimize microstructural alterations resulting from thermo-mechanical stresses induced by the cutting process.

Among the different shape memory alloy compositions, the near equiatomic NiTi alloys are by far the most widely-used shape memory materials for engineering applications [25]. The SME is the property of the material to recover mechanically induced strains when it is deformed in the low temperature phase (martensite) and subsequently heated up to the high temperature phase (austenite). This thermal change forces the return to the austenite and brings the SMA back to its original macroscopic shape. In the stress-free condition, the transformation from austenite to martensite, named forward transformation, occurs during cooling: it begins at the martensite start temperature M_s and ends at the martensite finish temperature M_f. Conversely, the reverse transformation, from martensite to austenite, occurs upon heating: this begins at the austenite start temperature A_s and ends at the austenite finish temperature A_f. These four temperatures are known as Transformation TempeRatures (TTRs).

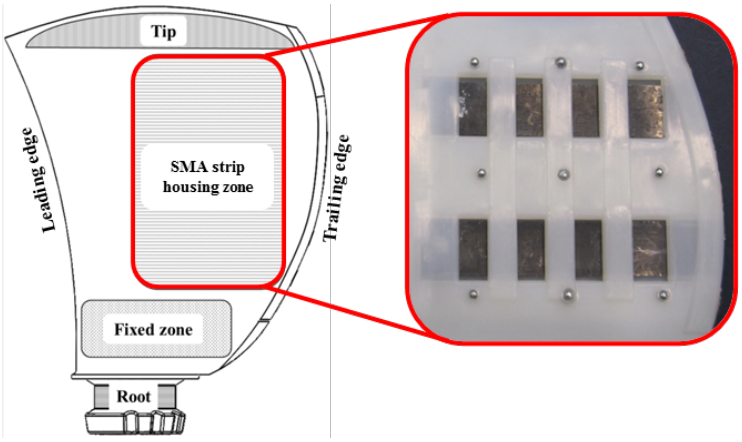

Figure 1 – Sketch of the SMA-based blade with its principal regions: root, fixed zone, SMA strip housing zone and tip. SMA strip housing zone allows the direct contact between SMA strips and airflow, as shown in the close-up.

As an inherent property of the material, SMA shows the One-Way Shape Memory Effect (OWSME) whereby they could recover large strains when deformed in the martensitic phase and heated above A_f. In addition to the OWSME, SMAs can exhibit, through specific thermo-mechanical treatments, the Two-Way Shape Memory Effect (TWSME). The TWSME behavior enables the macroscopic shape change upon heating and cooling without any external applied load. As a result, the material is able to spontaneously recover the memorized hot and cold shapes. Unfortunately, to induce the TWSME a tailored thermo-mechanical cycling must be applied and tuned for the specific application under a designed loading path [25].

According to the standard ASTM F2004, Differential Scanning Calorimetry (DSC) tests, by means of a TA Instruments DSC Q2000, were carried out on a small fraction of the untreated material. A constant heating/cooling rate of 10 °C/min was set for the DSC measurements. This thermal gradient is comparable with the actual thermal gradient of the automotive cooling circuits allowing material characterization in the working condition.

The characteristic TTRs were extrapolated from the DSC thermogram [26] through the tangential line method [25]. The obtained experimental values are summarized in Tab. 1. TTR data were the starting point for the development of the shape setting treatment, described as follows.

Table 1 − TTRs of SMA material in the untreated condition.

Austenite start temperature (A_s)	10 °C
Austenite finish temperature (A_f)	57 °C
Martensite start temperature (M_s)	48 °C
Martensite finish temperature (M_f)	-4 °C

SMA strip shape setting. In order to delete any residual stress of previous deformation history, the samples were first placed in a tube furnace and annealed at 700 °C for 20 min followed by controlled cooling to room temperature. The development of the best thermo-mechanical treatment for memorizing the defined bent shape was carried out experimentally. Temperature and time parameters were chosen according to the results of a previous study, where it was found experimentally that heating the material at 450 °C for 25 min allowed 92 % shape recovery [28]. Thus, after annealing, the strips were first strained in the martensitic state, by immersion in a propylene glycol bath cooled to -15 °C, and wound on a cylindrical jig to reach a circular shape. This setup was then placed into the tube furnace in constrained conditions, in order to avoid shape recovery on heating. To memorize this first shape, the material was heated at 450 °C for 25 min and subsequently quenched in the propylene glycol bath cooled to -15 °C. After this treatment, the strips were strained in the martensitic state again, applying opposite bending couples acting at the ends, locked into a specifically-designed arc clamp and thermally treated again at the aforementioned temperature and time conditions. Finally, by applying a uniform bending load, the strips were strained to a flat shape to be embedded in the blade structure. More details and the diagram of the performed thermo-mechanical treatment can be found in [26].

Polymeric structure selection. As a result of their good mechanical properties, which include high strength and stiffness to weight, good elongation and impact resistance, thermoplastic polymers are particularly suitable for engineering components and applications. Among them, Nylon PA66 is the most widely-used in the automotive industry, thanks to its versatility, moldability and resistance to high temperatures and harsh chemicals. Moreover, it is common practice to add glass fiber reinforcement to improve stiffness, strength and high temperature properties, or an elastomeric phase to increase the toughness of the thermoplastic matrix.

Given that the injection molding process was chosen for the manufacturing of the blade structure and according to the most widely-used polymeric matrices in fan blade production, the following materials were considered in this study: (i) Nylon PA66, (ii) two polymeric mixtures of Nylon PA66, glass fibers and elastomer and (iii) an acetal resin. The different polymeric compounds were compared considering: (i) an unreinforced Nylon PA66 named Compound A, (ii) a glass fiber reinforced Nylon PA66 (containing 15 % glass reinforcement) and 5 % elastomer named Compound B, (iii) a glass fiber reinforced Nylon PA66 (containing 25 % glass reinforcement) and 5 % elastomer named Compound C and (iv) an acetal resin named Compound D. Some properties of the polymeric compounds are summarized in Tab. 2.

Table 2 – Properties of polymeric compounds.

Property	Compound			
	A	B	C	D
Tensile Modulus [GPa]	1.49	3.89	6.13	3.1
Flexural Modulus [GPa]	1.40	3.51	5.14	2.90
Density [g/cm^3]	1.14	1.23	1.28	1.42

EXPERIMENTAL SETUP

An experimental apparatus, named Single Blade Test Facility (SBTF), including numerous temperature sensors, velocity sensors and digital image devices, was specifically designed to characterize the morphing blade.

SBTF. As depicted in Fig. 2, the SBTF was composed of (i) a convergent device, (ii) a polyvinyl chloride (PVC) pipe, (iii) a flow straightener, (iv) a polymethyl methacrylate (PMMA) transparent measurement section and (v) an exhaust pipe. The wind tunnel was driven by an axial fan with a nominal 1,500 m^3/h flow rate that provided the airflow through a 22 kW-electric heater. With the SBTF it was possible to create a highly-reproducible time-wise thermal gradient, capable of reaching values of up to about 12 °C/min in heating mode and up to about 6 °C/min in cooling mode. These temperature gradients are consistent with the operating conditions of fans when used normally.

Several calibrated thermocouples were installed in the SBTF to control the airflow temperature. They were placed close to the heater, near the blade (at the shroud and hub positions) and at the outlet section, as can be seen in the scheme of Fig. 2. Type K welded tip thermocouples were also placed on the blade surface and on the SMA strips to acquire the temperature trends during the activation tests.

Fig. 2 reports the experimental temperature evolution as a function of time, in the sections illustrated in the diagram. In order to control the thermo-fluid dynamic parameters of the airflow that hit the blade surface, it was essential that the PMMA panels were not removed during the test. For this reason, a conventional 3D scanner, such as a laser scanner or contact touch probe, could not be used. At the same time, such devices are usually unsuitable for real-time applications.

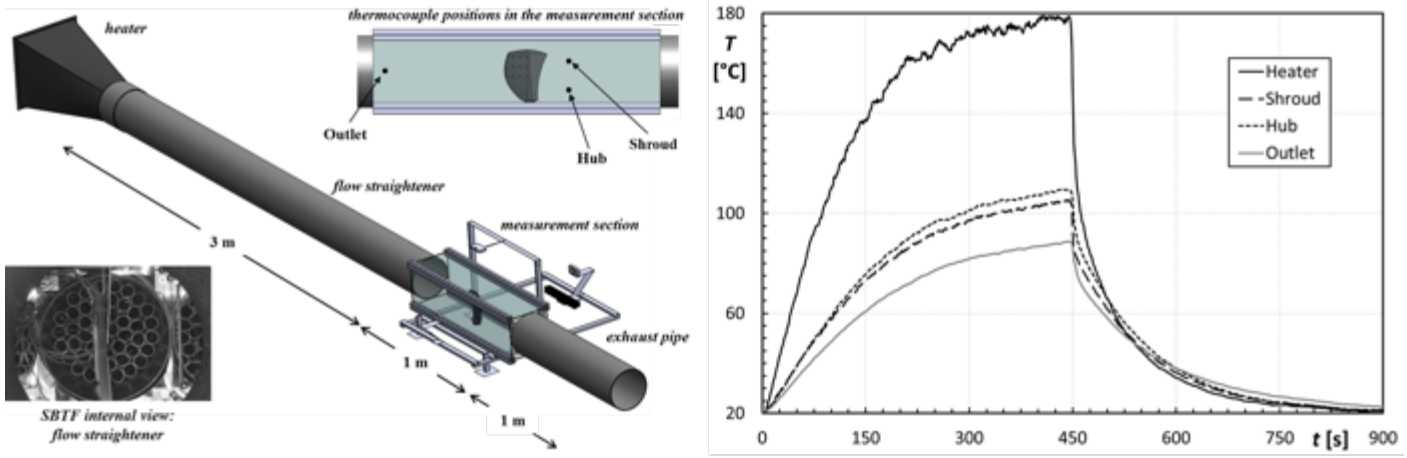

Figure 2 – Overall representation of the SBTF arrangement: heater, flow straightener, measurement section and exhaust pipe. The thermal performance are related to the measurement position indicated in the diagram of the measurement section.

Blade shape detection. Thanks to the transparency of the section of the measurement, the evolution of the blade shape was continuously evaluated by means of (i) digital image analysis and (ii) non-contact 3D shape measurement techniques. The blade shape scan and image acquisitions were synchronized with the temperature in order to control the shape changes related to the temperature trend.

As regards the digital image analysis, the evolution of the shape was continuously recorded during the activation cycle by means of video acquisition. Three digital cameras were aligned at the blade tip, suction side and pressure side, respectively. The camera arrangement used for the video acquisition measurements is given in Fig. 3. The camera aligned with the blade tip at a distance of 300 mm (camera A in Fig. 3) enabled the airfoil camber deflection to be detected. The camera aligned with the suction side, placed at a distance of 600 mm from the convex blade surface (camera B in Fig. 3), enabled the blade shape modification to be detected along its height. Furthermore, blade shape modification along the blade height was also detected by camera C placed close to the concave blade surface at a distance of 200 mm. The camera arrangement and settings allow spatial resolution up to 0.16 mm.

In addition to 2D video acquisition, the 3D blade shape was acquired during the tests using the Kinect sensor, which is capable of providing streaming non-contact depth information and color information at a resolution of (640 × 480) pixels with a rate of 30 frames per second. In this study, the ability of the Kinect sensor was exploited to acquire the shape changes upon activation of the blade placed behind the PMMA transparent panel. As depicted in Fig. 3, the Kinect was placed with the IR emitter axis perpendicular to the suction side blade surface (aligned with camera B and camera C), at a distance of 600 mm.

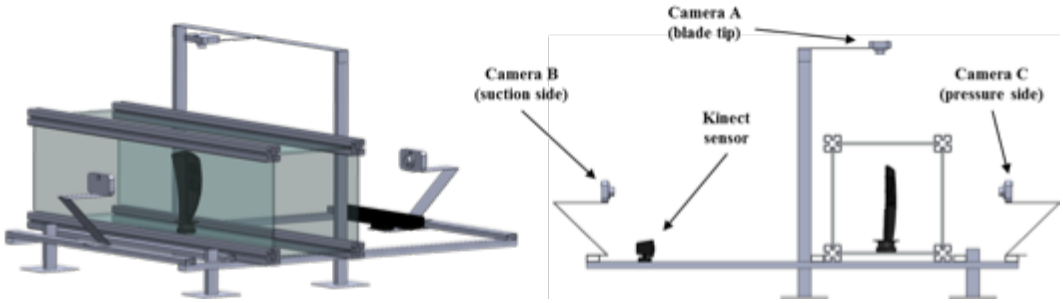

Figure 3 – Experimental setup for measuring 2D and 3D blade shape modification: isometric view and lateral view. The four detection devices (three digital cameras and the Kinect sensor) are aligned with the blade lateral surface and the blade tip.

Blade activation. The SMA thermal activation was achieved by (i) a heating ramp and (ii) a cooling ramp, which are described below. Starting at room temperature, the blade was first heated by hot airflow from the fan and electric heater, and was subsequently cooled down to room temperature when the heating system was switched off.

Figure 4 reports the temperature trends measured using the welded tip thermocouples for the polymeric structure and SMA strips. Given that uniform thermal conditions of the airflow and high-reproducibility of the temperature trend on the blade were achieved by the SBTF, the depicted trends are representative of all the considered polymeric matrices. As can be seen from Fig. 4, the temperature gradients in both the polymeric matrix structure and the SMA strips are quite similar and the blade shows an almost uniform surface temperature pattern. From Fig. 4 it is possible to note that the temperatures measured for the SMA strips (SM1, SM2, SS1 and SS2) are very similar to each other and for this reason, in the following analysis, the SMA strip temperature refers to the average values of these four measurements. The average value of the airflow temperature measured in the hub and shroud positions (see Fig. 2) is reported in Fig. 4 by using grey diamonds.

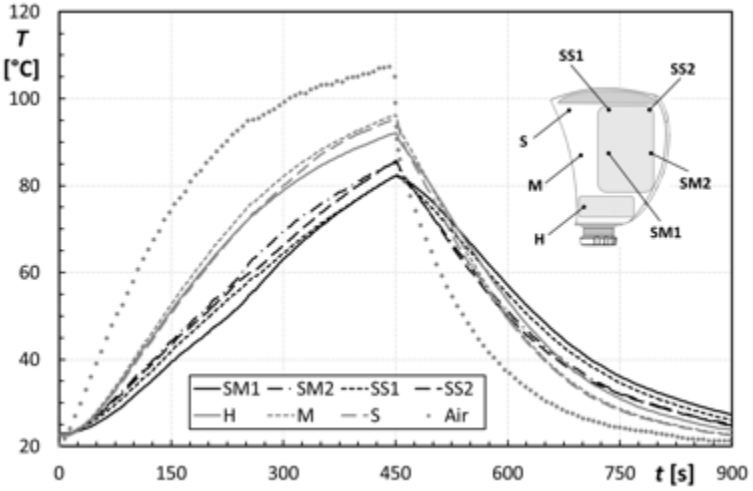

Figure 4 – Representative temperature trends for the polymeric structure (H, M and S) and SMA strips (SM and SS).

FUNCTIONAL STRUCTURE COMPARISON

The four polymeric compounds were compared by means of digital image analysis techniques. Quantitative analysis was performed to study tip blade deflection achieved by the shape recovery of SMA strips. The analysis was made taking into account the maximum distance m (maximum camber) from the chord length (leading edge to trailing edge line), as shown in Fig. 5. This distance was measured by means of CAD software reconstruction of the tip blade deflection, starting from the video frames recorded by the camera aligned with the blade tip (camera A, see Fig. 3). In particular $m_{\text{non-def}}$ corresponds to the maximum camber at the initial condition before the first activation cycle while m_i corresponds to the maximum camber at the i^{th} instant during the thermal cycle.

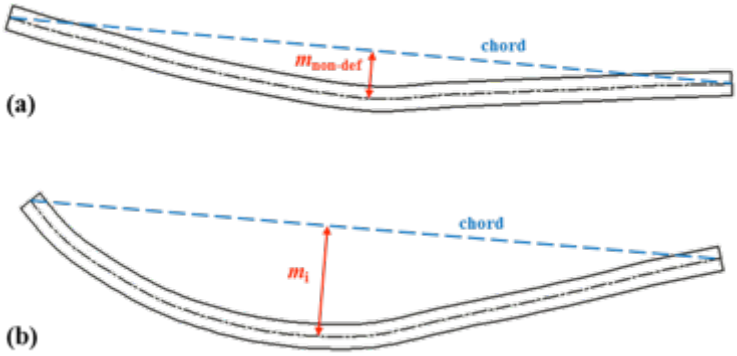

Figure 5 – Blade tip CAD reconstruction and measurement criterion: (a) maximum camber at the initial condition (room temperature) and (b) maximum camber at the i^{th} instant (activated).

In Fig. 6, blade deflection, calculated as $(m_i - m_{\text{non-def}})/ m_{\text{non-def}}$ as a function of the average strip temperature is proposed for the heating ramp as well as for the cooling ramp. As can be seen, the blade deflection increased during heating, reaching the maximum value at the maximum temperature. Given that the SMA thermally activated phase transformation does not occur instantly, a progressive and continuous increase in the deflection is observed. Note that, for all the polymeric compounds and SMA strip couplings, the effects of the phase transformation inside the strips appear at about 45 °C, given the presence of the polymeric structure constraint. It is well-known that the TTRs increase, with respect to the stress-free condition, when a mechanical load is applied (see Tab. 1). According to the different mechanical properties of the polymeric compounds reported in Tab. 2, the blade deflection trends are closely related to these features. In particular, Compound A (flexural modulus = 1.40 GPa) shows the steepest ramp, as a result of the minimum flexural modulus value. Conversely, Compound C (flexural modulus = 5.14 GPa), which had the greatest amount of glass reinforcement, showed a very low deflection. The large addition of glass fiber reduced the functional structure deflection capability on heating. Consequently, Compound B showed a behavior between Compound A and Compound C. These experimental findings are consistent with the mechanical properties and showed the strong influence of glass fiber reinforcement on blade shape modification. Finally, Compound D exhibited a blade deflection evolution very similar to that of Compound B, since the flexural modulus of these two polymeric matrices is quite comparable. Since the morphing blade takes advantage of the One-Way Shape Memory Effect (OWSME), during subsequent cooling the recovery behavior was achieved by the polymeric compound elasticity in conjunction with the SMA forward transformation.

When considering the blade deflection as a function of the average strip temperature for the cooling ramp, Compound A shows increased deformation instead of decreased temperature. This phenomenon could be due to over deformation during the heating ramp (see the steepest deformation trend), which caused the plastic deformation of the blade structure. Thus, the large blade deflection for Compound A proved that, for the intended functional structure application, the flexural modulus of unreinforced Nylon PA66 is too low. On the contrary, for the other compounds, the decrement of the blade deflection is consistent with the cooling ramp. In detail: (i) Compounds B and D showed almost the same recovery trend, which also occurred for the heating ramp and (ii) Compound C showed an almost horizontal recovery trend. As a result, Compounds B and D appear to be the most suitable polymeric matrices for the development of the blade structure coupled with the SMA strips.

The average temperature gradient trends for the heating and cooling ramps are also reported in Fig. 6. The airflow modification and then the modification of the temperature gradient trend are clearly visible starting from 45 °C at which the blade deflection caused flow disturbance and a different airflow field around the blade. Instead, in the cooling mode, the average temperature gradient is less steep and the flow disturbance is much less evident because blade deflection during recovery is more gradual compared to that of the heating ramp.

In order to highlight the differences between the polymeric compounds, in Fig. 6, the four blade tip image acquisitions are reported at (i) the instant at which the average strip temperature reached the peak value (deflection at peak temperature) and (ii) the

end of the thermal activation cycle (residual deflection). The difference in the camber variation among the four structures is a consequence of the trailing edge deflection, while at the leading edge, the blade tip shape modification is less pronounced even though the leading edge deformation is remarkable in the case of Compound D. Blade deflection in terms of (i) deflection at peak temperature, (ii) residual deflection and (iii) blade structure recovery are summarized in Tab. 3. The latter term is calculated by the difference between deflection at peak and residual temperature. The blade structure recovery values reported in brackets refer to the blade structure recovery divided by the maximum value. Starting from the values reported in Tab. 3, the best polymeric compound for this specific application is Compound B. This polymeric structure coupled with the thermally treated SMA strips shows the best compromise between the value of deflection at peak temperature and the capability of recovery. As a result, Compound B was chosen as the matrix for the blade structure and its deflection capability was evaluated through repeated thermal cycles.

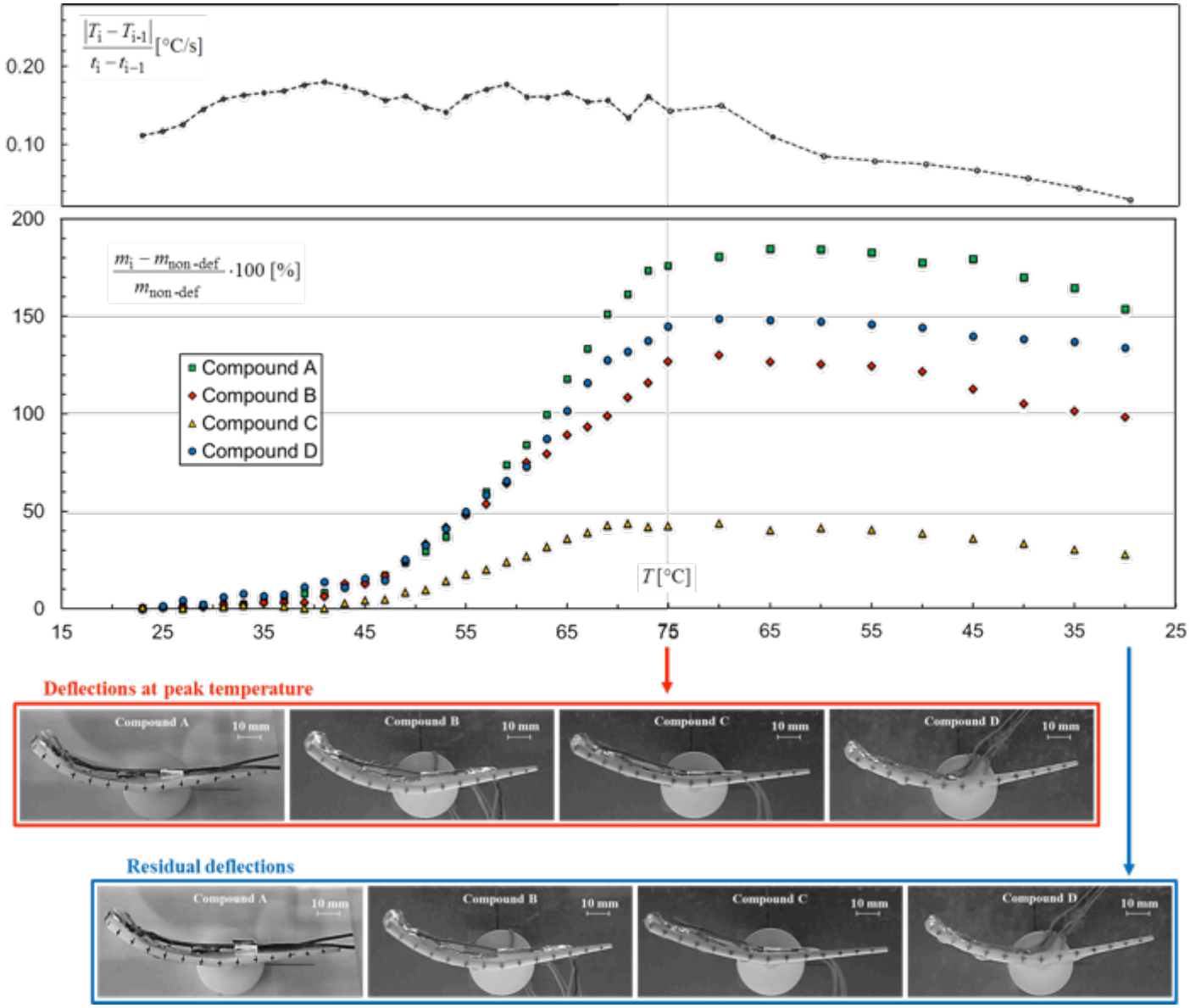

Figure 6 – Camber deformation for the four polymeric compounds during the heating ramp and cooling ramp and digital captures from the recorded video at the blade tip view for the deflections at peak temperature and the residual deflections.

Table 3 – Comparison of blade deflections.

Deflection	Compound			
	A	B	C	D
Peak Temperature [mm]	17.6	20.1	14.3	17.0
Residual [mm]	16.0	18.5	12.8	15.6
Blade structure recovery [mm]	1.6 (0.09)	1.6 (0.08)	1.5 (0.105)	1.4 (0.08)

Compound B stabilization. In order to study the effects of cyclic activation on the thermo-mechanical response of the SMA strips, the morphing blade was subjected to consecutive transformation cycles. It should be pointed out that the first thermal cycle corresponded to the first thermal cycle of the polymeric matrix and the SMA strips. The analysis is proposed for (i) the airfoil camber at peak temperature and (ii) the airfoil camber at the end of the activation cycle. The shape changes were evaluated by the CAD reconstruction, provided by using the digital images acquired during the activation tests at the blade tip view. Figure 7a reports the trend of the airfoil camber at peak temperature during the activation tests. The experimental results highlight that the blade stabilization in the activated condition is obtained from the 2nd activation test, in which the maximum camber is equal to about 21 mm, compared to a camber value of 9 mm that characterizes the blade tip airfoil in the initial condition. The variation in the maximum camber value is less than 1 mm. To study the capability of the blade to recover the same shape at the end of the thermal cycle, the residual deflection values are depicted in Fig. 7b. Experiments reveal that SMA strip displacement results in a camber variation equal to about 3 mm for each thermal activation cycle. Even though the variation of the residual deflection values is less than 0.5 mm, the residual deflection trend tends to get closer to the maximum camber trend. Therefore, the ability of the SMA strips to induce blade deflection progressively decreases as the thermal cycles increase.

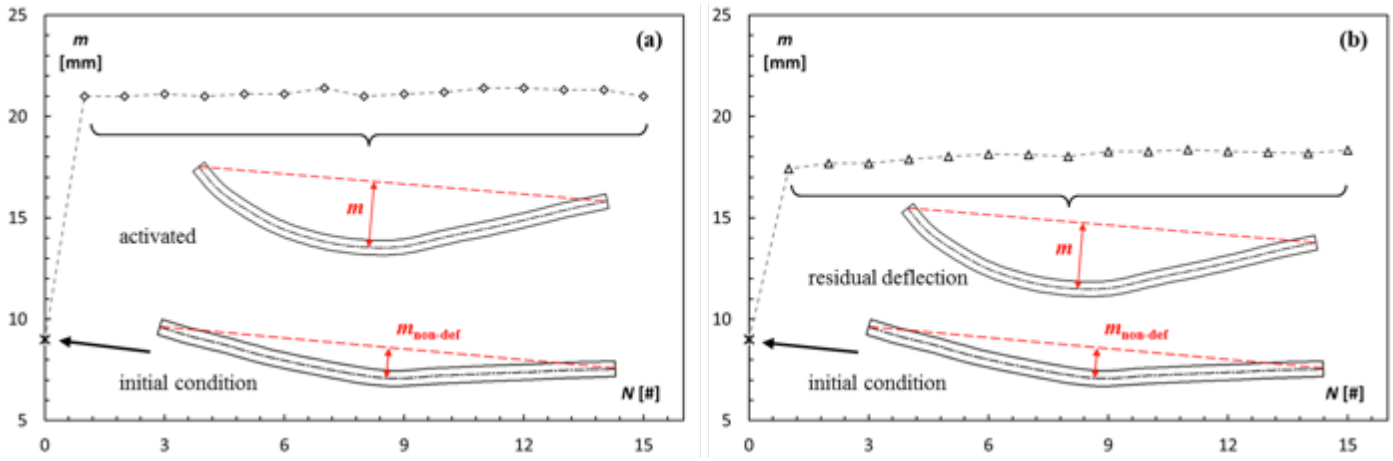

Figure 7 – Blade structure evolution: (a) airfoil camber at peak temperature and (b) residual deflection. The values are measured by means of CAD reconstruction.

MORPHING ANALYSES

Since the evaluation of the blade shape is fundamental for the overall comprehension of the SMA strip action as well as for the modification of the cooling fan performance, a detailed blade shape analysis was carried out. Due to its wide field of application, shape analyses of static and dynamic objects with non-contact shape techniques represent a hot topic. Considering the 3D surfaces, the shape measurement techniques are concerned with detecting the geometry information from the image of the measured object. These approaches are known in literature as Reverse Engineering (RE). RE is usually used for the reconstruction of an object of which the geometry is composed of several surfaces with different shapes. In the present application, the geometry is not composed of different parts, but the blade is positioned in the measurement section and a non-contact method (optical) must be used. As reported in [28], optical methods can often acquire more data in less time, with the advantage of measuring parts without contact. However, the scanning result may not achieve high level of accuracy and may have a higher uncertainty when compared to tactile systems [29]. In order to address these issues, the combination of optical measurements and tactile systems, even at different times and locations, can yield a highly accurate 3D representation of the physical object [30, 31]. In the present study, tactile systems cannot be used and for this reason, blade shape detection was carried out by means of (i) digital image analysis (that provides quantitative and accurate blade detection) and (ii) optical scanning (that provides qualitative blade detection).

The comparison will highlight (i) the modification of the blade shape during consecutive activation cycles and (ii) the capability of different non-contact methods of detecting and recognizing the blade shape modifications. Thus, starting from the results reported in Fig. 7, in the following sections the authors propose extensive two-dimensional and three-dimensional analyses of the blade shape modification that occurs in the 1st and 15th thermal cycle.

Two-dimensional analysis. The blade tip superimposition between the initial shape and maximum deflection for the 1st and 15th activation cycle are reported in Fig. 8. The values of the deviation between the initial blade shape and the maximum deflection, occurring at peak airflow temperature, were obtained by the marker points drawn on the tip. Superimposed black vectors join the same marker from the initial condition (black marker) to the activated condition (red marker). In this way, deviation intensity and direction are easily recognizable. The reported values represent the length of the vector in mm.

In more detail, the superimposition created for the 1st activation cycle shows that blade deformation occurs along the entire airfoil chord, while for the 15th activation cycle, blade deformation is localized only on the ends of the airfoil chord. The deformation imposed by the SMA strips during the 1st activation thermal cycle implies significant modification of the airfoil meanline. The polymeric blade structure is not able to fully recover this meanline modification; in fact, in the blade tip capture realized for the 15th activation cycle, the SMA strip activation induces blade shape modification only in the leading edge and trailing edge regions. The ability of the SMA strips to induce blade deformation decreases as a function of the number of activation cycles (as reported in Fig. 8) and the modification is increasingly localized at the end of the airfoil.

In addition to blade tip analysis, by using the digital images acquired by the suction side camera (see Fig. 3 for the camera arrangement), the blade shape modification along the blade height can be studied. Given that any 3D curved surface could be represented through Cartesian coordinates, the blade shape modification was analyzed in this way. To determine the coordinate variation with the shape evolution, a suction side video acquisition was considered since the welded tip thermocouples placed on the pressure side prevent the detection of the whole blade surface. Thanks to a regular pattern depicted on the suction side of the blade surface, the comparison between the shapes at (i) initial condition and (ii) deflection at peak temperature were taken into account.

In the same way as the blade tip analysis, Fig. 9 reports (i) superimposition between the initial shape and deflection at peak temperature for the 1st and 15th thermal cycle and (ii) the values of the deviation between the initial blade shape and the deflection that occurs at peak airflow temperature. With the same strategy, superimposed black vectors join the same marker from the initial condition (black marker) to the activated condition (red marker). It is possible to observe that during the 1st activation cycle, the blade shape changes in the leading edge and trailing edge regions (Fig. 9). For the 1st cycle, significant deviation can be found in the trailing edge region where the difference reached the value of 2.5 mm. Conversely, at the 15th cycle SMA strip activation can change only in the trailing edge region, and the deviation reaches only 0.6 mm. Unlike the view of the blade tip reported above, in the leading edge zone the deviation is not noticeable by using suction side image acquisition.

Thanks to the analyses reported in Figs. 8 and 9, it is possible to note that the blade shape changes according to the SMA strips and the actions of the polymeric structure. In particular, the blade shape is concave (moves towards the pressure side) both in the leading edge and trailing edge regions. This phenomenon, clearly depicted in Fig. 8, occurs with different intensity along the blade height. In fact, as reported in Fig. 9, the values of the deviation are different from the hub to the tip. In particular, the deviation is the lowest in the regions close to the root, while the deviation assumes the highest values in the SMA strip housing region.

From these results it is easy to understand that, in order to recognize the actual blade shape during SMA strip activation, different methods have to be taken into account. The 2D image analysis techniques could represent suitable tools for measuring 2D deviation (and thus blade structure deformation) in a very accurate way. However, this method does not permit an overall evaluation of the blade shape. Because of the limitation of the 2D image analysis, 3D blade detection is proposed in the final part of this work.

Three-dimensional analysis. The instantaneous 3D blade shape was acquired during the tests by using the Kinect sensor that allowed the digitalization of the blade shape. By using 3D detection, it is possible to (i) evaluate the blade shape changes during the activation tests and (ii) reconstruct the 3D blade shape by using a CAD modeler.

In the first step, the Kinect sensor through the SDK Software Development Kit toolkit was set depending on the measurement range, the required resolution, the specific levels of environmental light, and the surface appearance of the object. In this preliminary phase, the blade surface was prepared in order to avoid reflection by using a specific spray. The detection consists of blade shape digitalization by using the point cloud data provided by the SDK tool. The point cloud elaboration was performed by means of open source software (i.e. Blender, MeshLab) and the .stl file with the blade surface mesh was generated.

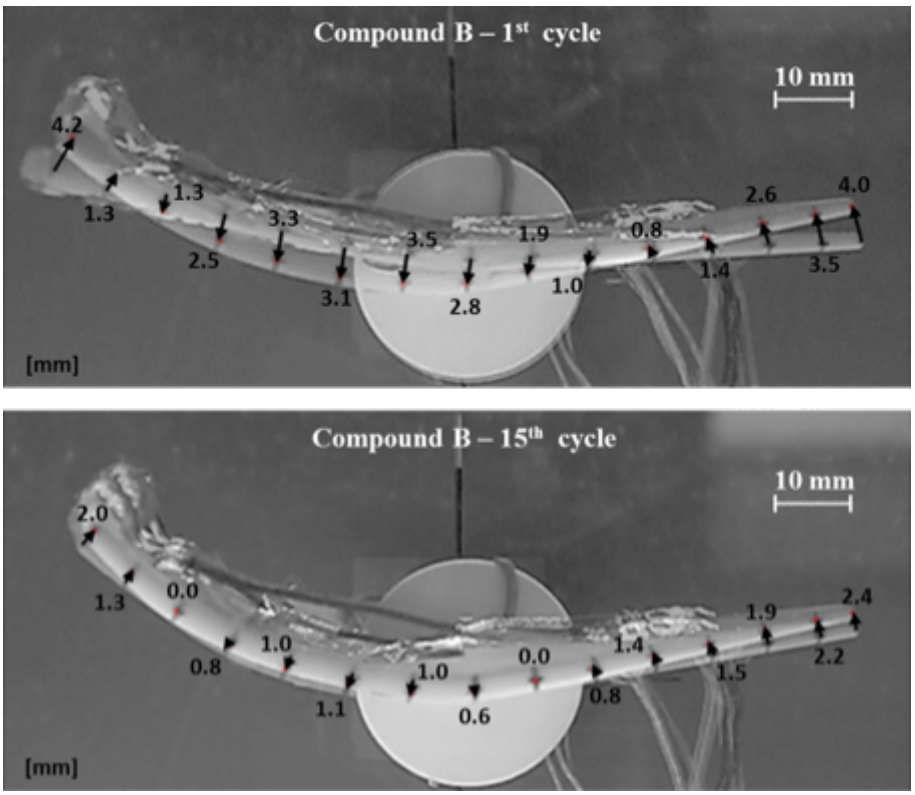

Figure 8 – Two-dimensional blade tip comparison. Blade tip superimposition between the initial shape and the maximum deflection for the 1st and the 15th activation cycle.

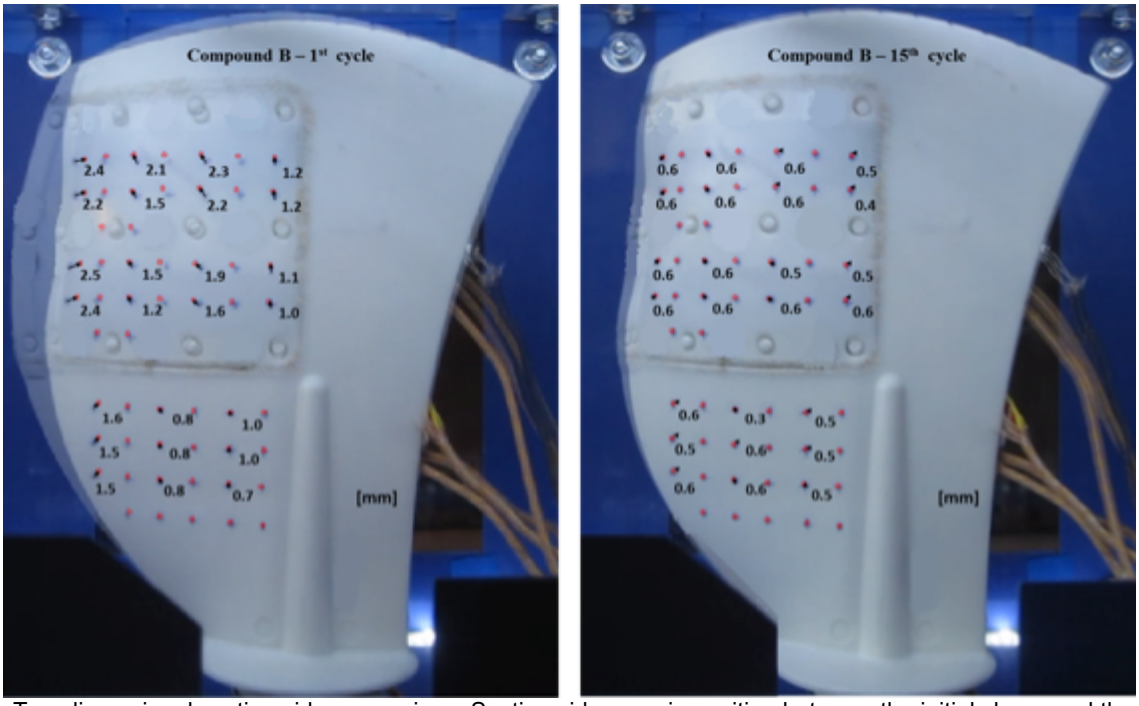

Figure 9 – Two-dimensional suction side comparison. Suction side superimposition between the initial shape and the maximum deflection for the 1st and the 15th activation cycle.

Point cloud data were then processed and converted into a polygonal representation of the scanned blade. The treatment of the point cloud is comprehensive of: (i) filtration in order to reduce the noise level, (ii) reduction of the mesh size through the elimination of the verbatim point, (iii) local modification of the mesh in order to fill the hole (if present) and make the surface as regular as possible and, finally, (iv) creation from the triangle mesh of the NURBS-based CAD model of the blade.

In order to validate the ability of the Kinect sensor to acquire the 3D blade shape, a preliminary comparison between the blade reference CAD geometry and the acquired Kinect surface was conducted. In Fig. 10, the acquired surface of the blade at the initial condition and the blade CAD geometry are superimposed. As shown, the Kinect sensor provided an accurate 3D blade shape since the two entities only differed at the boundary blade regions (especially at the blade tip), where the deviation was less than 1 mm. At the edges, the Kinect sensor also detected the blade thickness (as can be seen in Fig. 10), but this detection is less accurate and it is not taken into account during the blade shape analysis and the following reconstruction.

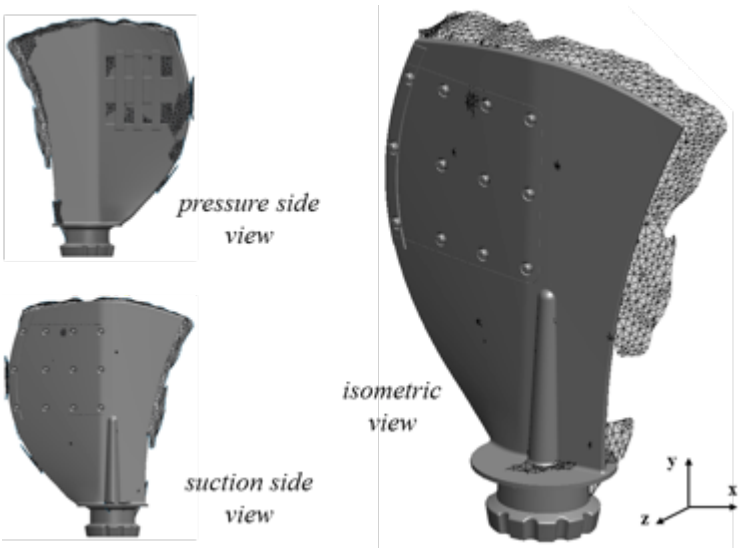

Figure 10 – Blade shapes comparison: raw Kinect surface vs CAD geometry. Three views: pressure side, suction side and isometric.

As stated above, the Kinect sensor was used to instantly detect the 3D blade shape during the activation test at (i) the start of the thermal cycle and (ii) the end of the heating ramp at peak temperature. The detections reported in Fig. 11 refer to the 1st and 15th activation cycle. As can be seen, the maximum blade deflection located at the SMA strip housing zone (from 50 % to 87 % of the blade span, see Fig. 1) is clearly visible from the scanned surfaces. The deformations in the trailing edge area are highly noticeable even from the raw acquired surface.

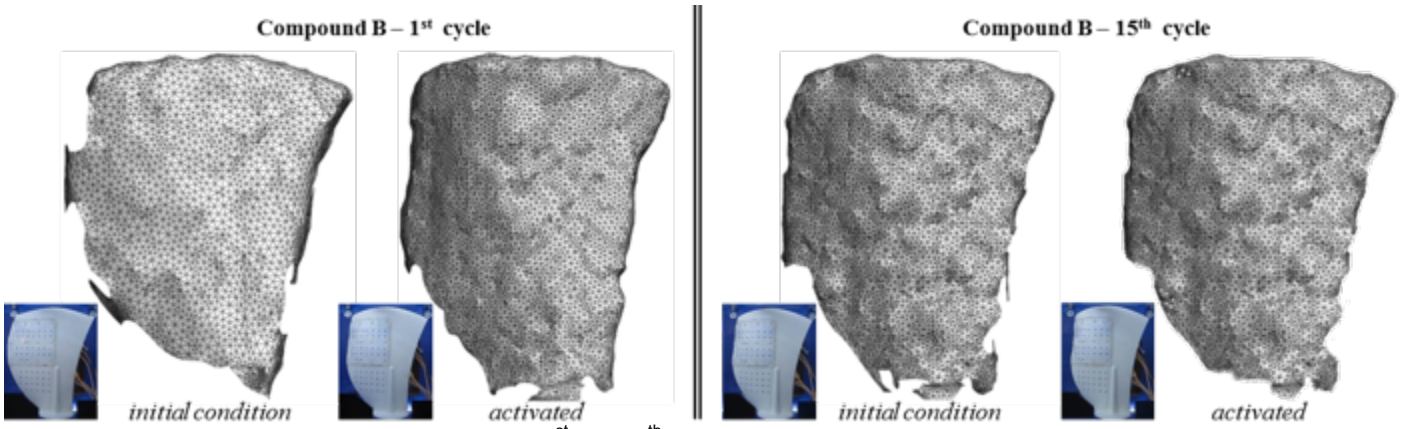

Figure 11 – Kinect surfaces for the 1st and 15th activation cycle in two conditions: initial and activated.

Thanks to the 3D surface provided by the Kinect sensor during the activation tests, it was possible to analyze the different deformations that occurred in the blade shape along its span in a quantitative way. Figure 12 reports the intersection between the suction side surface (Kinect surface) and the four different planes at increasing spans: 20 %, 50 %, 70 % and 90 % for a blade height

of 34.8 mm, 87.0 mm, 128.8 mm and 156.6 mm, respectively. The intersection is represented by circular and triangular single points for the initial condition and activated blade shape respectively, while the trend line improves the readability of the graph.

Since the SMA strip housing zone is located above the midspan, the intersection at 20 % of the span showed no differences between the two suction side surfaces. By contrast, the other intersections showed remarkable deviations among the surfaces. In the leading edge area the activated blade shows the deviation with respect to the initial blade shape only in the 1st cycle. This deviation is about 13 mm, 15 mm and 20 mm for 50 %, 70 % and 90 %, respectively. During the 15th cycle, the deviation in the leading edge area is very limited and it is hidden by the surface approximation. Conversely, in the trailing edge area the activated blades show a greater amount of deviation in both of the cycles. The deviation between the activated blades is more evident for the 70 % and 90 % intersections. As depicted in Fig. 12, blade shape changes (mean line deflection and trailing edge deformation) develop on each blade-to-blade plane (grey planes in Fig. 12) as a function of the blade span location.

It should be observed that progressive and continuous blade deformation, due to temperature-driven shape recovery, is directly related to the design of (i) the thermo-mechanical shape setting SMA strips, (ii) the position of the SMA strip housing zone and (iii) the polymeric matrix stiffness.

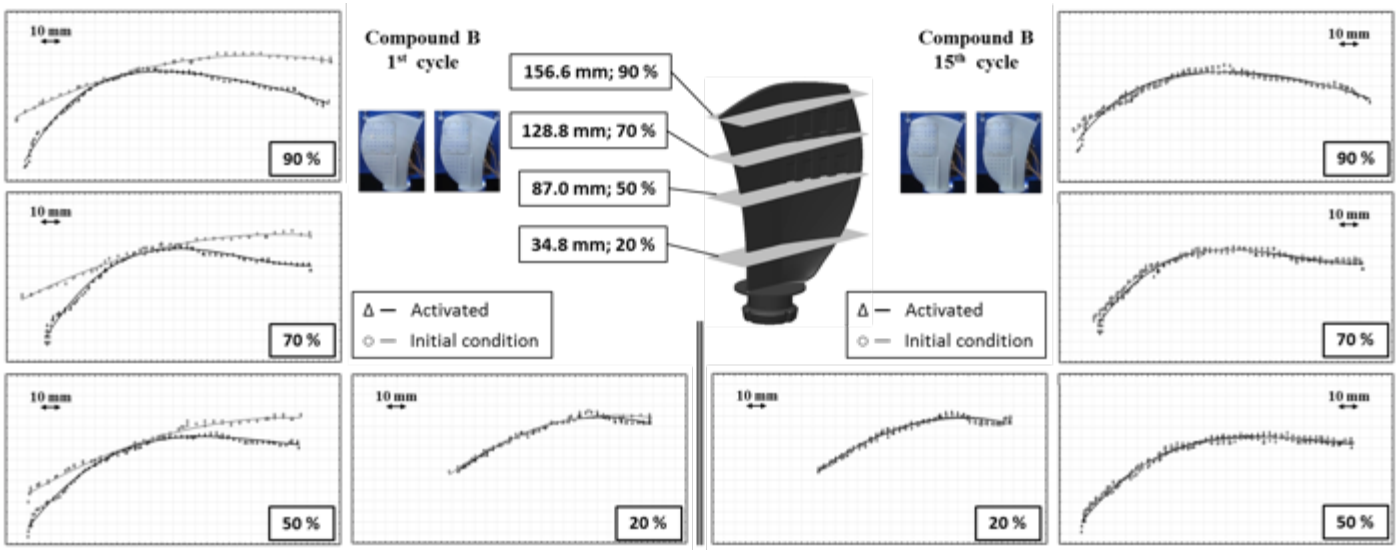

Figure 12 – Suction side deviations at 20 %, 50 %, 70 % and 90 % of the blade span for the 1st and 15th activation cycle in two condition: initial and activated. The grid size is in accordance with the dimensional bar.

Thanks to these accurate Kinect surfaces the corresponding 3D blade shapes can be achieved. The 3D analysis carried out by a non-contact device allows blade shape analysis in all of the blade sections. The 3D blade detection is less accurate (point clouds data generated by the Kinect sensor were affected by blade surface finishing and the reflection and diffraction of the PMMA panels) than the 2D image captured by a digital camera, but is highly suitable for detecting the instantaneous overall 3D blade shape without disturbing the airflow.

The reconstructed blades obtained through a reverse procedure starting from the Kinect surfaces are reported in Fig. 13. The parametric CAD representations were generated through B-Splines surface provided by SolidWorks CAD software. Therefore, through the accurate activation tests carried out in the wind-tunnel, in which the thermal conditions and the airflow are controlled and measured, it is possible to detect the actual blade shape and use this to improve both knowledge and functional structure performance by using numerical methods. The ability of this procedure to generate 3D blade shapes allows for the evaluation of the functional structure by using a numerical simulation such as FEM or CFD in conjunction with the experimental analysis.

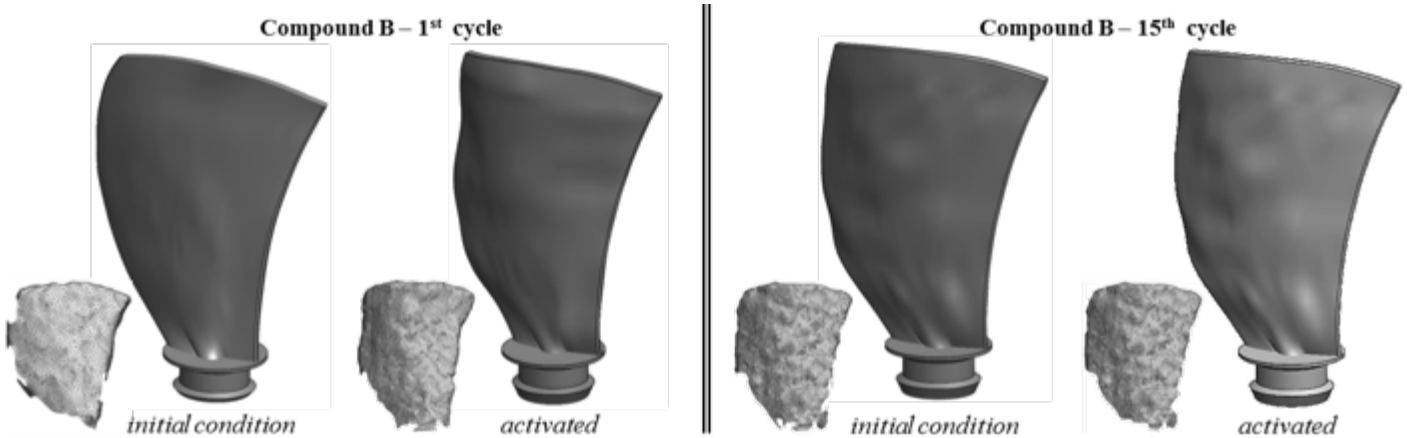

Figure 13 – Reconstructed blades for the 1st and 15th activation cycle in two conditions: initial and activated.

CONCLUSIONS

In this paper the development of a morphing blade via SMA strips activation has been proposed. The blade was designed as a functional structure with the active elements embedded in a polymeric matrix and placed in direct contact with the airflow. The intent to use embedded SMA elements refers to the design of a fan in which the blade shape changes continuously as a function of the airflow temperature. The main aim was to compare the four different polymeric compounds to establish the best compromise between their stiffness and deflection according to the application.

In order to reach the deflection of the blade structure on activation, the strips were thermo-mechanically treated by means of a double shape setting process, of which the parameters were experimentally tuned to maximize the shape memory effect. The thermal activation of the strips was performed by using a purpose-built wind tunnel that reproduced the actual automotive thermal ramps of the heat exchanger. The ability of the SMA strips to induce the blade deformation was studied by using both 2D and 3D techniques.

Considering the preliminary analyses performed in this work the following considerations can be made:

- The shape setting treatment allowed the shape memory effect to be maximized in order to generate the widest deflection of the blade structure.
- The comparison of the blade structures was carried out by means of 2D imaging and 3D non-contact techniques. The analyses showed the influence of the amount of glass fiber on the blade stiffness revealing that the decrease in the amount of glass fiber causes an increase in blade deflection during thermal activation.
- The SMA two-dimensional strip housing zone determines three-dimensional blade shape changes in a different way from the root to the blade tip; accordingly, only by using 3D blade detection is it possible to evaluate the actual blade shape modification. 3D blade recognition is less accurate than 2D image analysis but it provided overall and instantaneous information about the blade shape modification during the activation cycle without disturbing the airflow.
- The presence of glass fiber reduced blade deflection up to 20 % but promoted blade shape recovery. The glass fiber reinforced Nylon PA66 containing 15 % glass reinforcement and 5 % elastomer showed the best compromise and was thus chosen for the stabilization analysis. The maximum blade deflection was already reached by the 2nd cycle, even though the residual deflection showed an increasing trend during the overall stabilization procedure.

These experimental findings highlight the opportunity to generate an innovative passive control system applied to an automotive cooling fan. Future developments will concern (i) the study of a thermo-mechanical treatment to induce the Two-Way Shape Memory Effect on the SMA material in order to increase blade shape recovery, (ii) the study of the shape recovery behavior in subsequent activation thermal cycles to improve blade structure stabilization, (iii) the reliability of the non-contact detection method for the analysis of the blade shape modification in order to perform numerical analysis and (iv) the use of reconstructed blades (initial and activated condition) for structural and fluid dynamic analysis.

ACKNOWLEDGEMENTS

The authors wish to thank Fratelli Rosati s.r.l. of Leinì (Torino – Italy) for the financial and technical support in this research.

REFERENCES

[1] Tsoi KA, Schrooten J, Stalmans R. Part I. Thermomechanical characteristics of shape memory alloys. Mater Sci Eng, A 2004;368:286–98.

[2] Otsuka K, Wayman MC. Shape memory materials. Cambridge: Cambridge University Press;1998.

[3] Wei ZG, Sandstrom R, Miyazaki S. Shape memory materials and hybrid composites for smart systems: Part II Shape-memory hybrid composites. J Mater Sci 1998;33:3763–83.
[4] Zhou G, Lloyd P. Design, manufacture and evaluation of bending behavior of composite beams embedded with SMA wires. Compos Sci Tech 2009;69(13):2034–41.
[5] Sreekumar M, Nagarajan T, Singaperumal M. Application of trained NiTi SMA actuators in a spatial compliant mechanism: Experimental investigations. Mater Des 2009;30:3020–9.
[6] Song G, Kelly B, Agrawal BN. Active position control of a shape memory alloy wire actuated composite beam. Smart Mater Struct 2000;9:711–6.
[7] Icardi U. Large bending actuator made with SMA contractile wires: theory, numerical simulation and experiments. Composites Part B 2001;32:259–67.
[8] Baz A, Chen T, Ro J. Shape control of NITINOL-reinforced composite beams. Composites Part B 2000;31:631–42.
[9] Hartl DJ, Lagoudas DC. Aerospace applications of shape memory alloys. Proceedings of the Institution of Mechanical Engineers Part G: J Aerosp Eng 2007;221:535–52.
[10] Stanewsky E. Aerodynamic benefits of adaptive wing technology. Aerosp Sci Technol 2000;4(7):439–52.
[11] Calkins FT, Mabe JH. Shape memory alloy based morphing aerostructures. J Mech Des 2010;132(11)
[12] Bil C, Massey K, Abdullah EJ. Wing morphing control with shape memory alloy actuators. J Intell Mater Syst Struct 2013;24(7):879–98.
[13] Sun L, Huang WM, Ding Z, Zhao Y, Wang CC, Purnawali H, Tang C. Stimulus-responsive shape memory materials: a review. Mater Des 2012;33:577–640.
[14] Schick JR, Hartl DJ, Lagoudas DC. Incorporation of shape memory alloy actuators into morphing aerostructures. In: Valasek. *Morphing aerospace vehicles and structures*, United Kingdom: John Wiley & Sons; 2012, pp. 231–60.
[15] Coutu D, Brailovski V, Terriault P. Optimized design of an active extrados structure for an experimental morphing laminar wing. Aerosp Sci Technol 2010;14(7):451–8.
[16] Sofla AYN, Meguid SA, Tan KT, Yeo WK. Shape morphing of aircraft wing: status and challenges. Mater Des 2010;31:1284–92.
[17] Barbarino S, Bilgen O, Ajaj RM, Friswell MI, Inman DJ. A review of morphing aircraft. J Intell Mater Syst Struct 2011;22:823–77.
[18] Epps J, Chopra I. In-flight tracking of helicopter rotor blades using shape memory alloy actuators. Smart Mater Struct 2001;10:104–11.
[19] Daynes S, Weaver PM. A morphing trailing edge device for a wind turbine. J Intell Mater Syst Struct 2012;23(6):691–701.
[20] Lachenal X, Daynes, S, Weaver PM. Review of morphing concepts and materials for wind turbine blade applications. Wind Energy 2013;16:283–307.
[21] Strelec JK, Lagoudas DC, Khan MA, Yen J. Design and implementation of a shape memory alloy actuated reconfigurable airfoil. J Intell Mater Syst Struct 2003;14:257–73.
[22] Ponta FL, Otero AD, Rajana A, Lagoa LI. The adaptive-blade concept in wind-power applications. Energy Sustain Dev 2014;22:3–12.
[23] Weisshaar TA. Morphing aircraft systems: historical perspectives and future challenges. J Aircr 2013; 50(2):337–53.
[24] Oehler SD, Hartl DJ, Lopez R, Malak RJ, Lagoudas DC. Design optimization and uncertainty analysis of SMA morphing structures. Smart Mater Struct 2012;21(9):1–16.
[25] Lagoudas DC. Shape memory alloys: Modeling and Engineering Applications. Texas: Springer; 2008.
[26] Fortini A, Merlin M, Soffritti C, Suman A, Garagnani GL. Study of an active deformable structure with embedded NiTi shape memory alloy strips. La Metallurgia Italiana 2015;2(107):23–30.
[27] Rizzoni R, Merlin M, Casari D. Shape recovery behaviour of shape memory thin strips in cylindrical bending: experiments and modeling. Continuum Mech Termodyn 2013;25:207–27.
[28] Schwenke H, Neuschaefer-Rube U, Pfeifer T, Kunzmann H. Optical methods for dimensional metrology in production engineering. CIRP Ann-Manuf Technol 2002;51/2:685–99.
[29] Sansoni G, Docchio F. In-field performance of an optical digitizer for the reverse engineering of free-form surfaces. Int J Adv Manuf Technol 2005;26/Sep(11–12):1353–61.
[30] Carbone V, Carocci M, Savio E, Sansoni G, De Chiffre L. Combination of a vision system and a coordinate measuring machine for the reverse engineering of free-form surfaces. Int J Adv Manuf Technol 2001;17:263–71.
[31] Chen L-C, Lin GCI. An integrated reverse engineering approach to reconstructing free-form surfaces. Comput Integr Manuf Syst 1997;10:49–60.